J|A|C|S ARTICLES

Published on Web 01/22/2010

Quantitative Study of the Association Thermodynamics and Kinetics of DNA-Coated Particles for Different Functionalization Schemes

Mirjam E. Leunissen,*,†,‡ Remi Dreyfus,†,§ Roujie Sha,|| Nadrian C. Seeman,|| and Paul M. Chaikin†

Center for Soft Matter Research, Physics Department, New York University, 4 Washington Place, and Chemistry Department, New York University, 100 Washington Square East, New York, New York 10003

Received September 17, 2009; E-mail: m.e.leunissen@amolf.nl

Abstract: Surface functionalization with complementary single-stranded DNA sticky ends is increasingly used for guiding the self-assembly of nano- and micrometer-sized particles into larger scale ordered structures. Here we present measurements, formulas, and graphs that allow one to quantitatively predict the association behavior of DNA-coated particles from readily available Web-based data. From experiments it appears that the suspension behavior is very sensitive to the grafting details, such as the length and flexibility of the tether constructs and the particles' surface coverage. Thus, if one wants to control the interactions and assembly processes, insight is needed into the structural and dynamical features of the DNA coatings. We demonstrate how a straightforward measurement of the particles' association−dissociation kinetics during selected temperature cycles, combined with a simple quantitative model, can reveal the relevant properties. We used this method in a systematic study where we varied the temperature cycle, the bead concentration, the particles' surface coverage, and the DNA construct. Among other things, we find that the backbone that tethers the sticky ends to the surface can have a significant impact on the particles' dissociation properties, as it affects the total number of interparticle bonds and the configurational entropy cost associated with these bonds. We further find that, independent of the tether backbone, self-complementary "palindromic" sticky ends readily form intraparticle hairpins and loops, which greatly affect the particles' association behavior. Such secondary structure formation is increasingly important in faster temperature quenches, at lower particle concentration, and at lower surface coverage. The latter observations are especially useful for the design of so-called self-protected DNA-mediated interactions, which we pioneered recently and for which we expect to find an increasing use, as they enable more versatile assembly schemes.

Introduction

A large fraction of colloid science and nanoscience is aimed at the creation of ordered two- and three-dimensional particle assemblies with, for instance, novel optical and electronic properties (see for an example ref 1). Preferably, these materials are formed in a bottom-up fashion by spontaneous self-assembly of the particles, but at present the complexity of such self-assembled structures is still limited. The past decade, however, has seen a dramatic advancement in the programmability of the interactions between nano- and micrometer-sized particles through the use of biomolecules with selective recognition capabilities.[2−5] Surface functionalization with complementary, single-stranded DNA "sticky ends" [5] is especially appealing for guiding the particles to their designated neighbors,[6−10] because the DNA linkages are entirely temperature reversible. Moreover, the library of specific sticky ends is practically infinite by virtue of their readily programmable nucleotide sequence.

For cDNA oligonucleotides in solution it is well-known that the transition from the hybridized (or double-stranded) state at low temperature to the dehybridized (or single-stranded) state at high temperature depends on the sequence and number of base pairs, the oligonucleotide concentration, and the ionic

† Physics Department.
‡ Present address: FOM Institute for Atomic and Molecular Physics, Sciencepark 104, 1098 XG, Amsterdam, The Netherlands.
§ Present address: Complex Assemblies of Soft Matter, CNRS-Rhodia-UPenn UMI 3254, Bristol, PA 19007.
|| Chemistry Department.

(1) Urban, J. J.; Talapin, D. V.; Shevchenko, E. V.; Kagan, C. R.; Murray, C. B. *Nat. Mater.* **2007**, *6*, 115–121.
(2) Mann, S.; Shenton, W.; Li, M.; Connolly, S.; Fitzmaurice, D. *Adv. Mater.* **2000**, *12*, 147–150.
(3) Hiddessen, A. L.; Rodgers, S. D.; Weitz, D. A.; Hammer, D. A. *Langmuir* **2000**, *16*, 9744–9753.
(4) Lee, S. K.; Maye, M. M.; Zhang, Y. B.; Gang, O.; Van der Lelie, D. *Langmuir* **2009**, *25*, 657–660.
(5) Mirkin, C. A.; Letsinger, R. L.; Mucic, R. C.; Storhoff, J. J. *Nature* **1996**, *382*, 607–609.
(6) Tkachenko, A. V. *Phys. Rev. Lett.* **2002**, *89*, 148303.
(7) Biancaniello, P. L.; Kim, A. J.; Crocker, J. C. *Phys. Rev. Lett.* **2005**, *94*, 058302.
(8) Crocker, J. C. *Nature* **2008**, *451*, 528.
(9) Park, S. Y.; Lytton-Jean, A. K. R.; Lee, B.; Weigand, S.; Schatz, G. C.; Mirkin, C. A. *Nature* **2008**, *451*, 553–556.
(10) Nykypanchuk, D.; Maye, M. M.; van der Lelie, D.; Gang, O. *Nature* **2008**, *451*, 549–552.

strength of the buffer.[11] In addition to these factors, the interactions of DNA-functionalized particles also depend on the grafting details, such as the density of the sticky end coverage on the particle surface.[7,12−18] Also the polymeric properties of the grafted DNA can be exploited to influence the particle interactions and their self-assembled structures, for instance, through variation of the length and flexibility of the backbone constructs that tether the short sticky ends to the particle surface.[9,10,14,19−21] Experimentally, it appears that the suspension behavior is very sensitive to seemingly small changes in these grafting details. Furthermore, in ref 17 we have shown that the overall binding properties of the particles are strongly affected by the configurational entropy cost that is associated with the hybridization of tethered sticky ends and that depends on the details of the DNA functionalization.

Recently, we have introduced another feature that provides even more control over the particles' binding strength and association kinetics in the form of switchable self-protected interactions.[22] These novel interactions are based on the ability of single-stranded DNA to form well-defined folded (or secondary) structures, particularly hairpins, if some stretches of the nucleotide sequence are internally complementary. Also, if neighboring sticky ends on the same bead are complementary to each other, they can in principle form intraparticle "loops". In a fast temperature quench, these hairpin and loop structures form within microseconds inside the particles' DNA coatings, well before the beads encounter each other by diffusion (the diffusive time scale is seconds to minutes for micrometer-sized particles[23]). Consequently, at low temperature, the sticky ends are "self-protected" and particle association through the formation of interbead bonds is prevented. At high temperature, the secondary structures dehybridize and the particle association is reactivated, provided that the interparticle bonds have a sufficiently large binding energy. Figure 1 illustrates the basic principle with an experiment in which we monitored the fraction of nonassociated particles, or the singlet fraction, while we cycled the sample temperature up and down. In ref 22 we have shown that such switchable self-protected interactions can greatly extend the utility of DNA-functionalized systems, as they provide additional kinetic control over the particle interactions and allow for more versatile, multistage assembly approaches.

In all of the aforementioned cases, a good insight into the structural and dynamical properties of the DNA coatings is required if we want to have a fine control over the particles' interactions and their assembly process. In the present paper, we show how carefully chosen temperature cycles can be used as a simple diagnostic tool that reveals some of the main structural−dynamical characteristics of the tethered DNA constructs. Together with the theoretical model that we develop here, this provides quantitative insight into the competing interparticle and intraparticle hybridization events, the associated configurational entropy costs, and the association and dissociation kinetics of the particles. In this way, we systematically study the suspension behavior as a function of the temperature quench rate, the bead concentration, the sticky end coverage, and the type of DNA construct. We compare constructs with single- and double-stranded tether backbones, with normal Watson−Crick or self-complementary palindromic sticky ends, and with or without the ability to form secondary structures, such as hairpins and intraparticle loops.

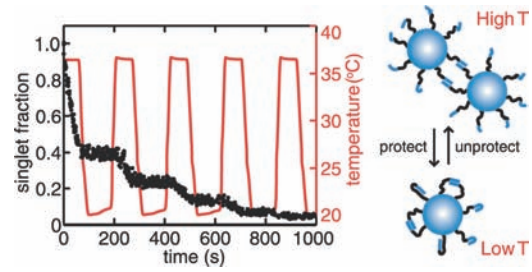

Figure 1. Repeated switching of self-protected interactions. By cycling the temperature (shown in red) below the dissociation temperature of the DNA-functionalized beads, the sticky ends are repeatedly protected (low temperature) and unprotected (high temperature) through secondary structure formation. This switches the particle association alternatingly off and on, leading to a stepwise decrease in the particle singlet fraction (black dots). The particles were functionalized with a self-complementary palindromic sequence that could form both hairpins and loops.

Theoretical Model

In this section, we will derive expressions for the binding free energy of DNA-functionalized particles as well as the parameters that describe the particles' association and dissociation kinetics, which we will then use to model the suspension behavior.

Hybridization Free Energy of Tethered DNA. Our starting point is the equilibrium between a pair of complementary single-stranded DNA molecules (A, B) and their double-stranded hybridization product (AB):

$$\mathrm{A} + \mathrm{B} \rightleftharpoons \mathrm{AB} \tag{1}$$

The partition function for N_x molecules of species x = A, B, or AB at temperature T can be written as

$$Z_x(N_x, V_x, T) = \frac{V_x^{N_x}}{\Lambda_x^{3N_x} N_x!} z_{\mathrm{int},x}^{N_x} \tag{2}$$

where $\Lambda_x = (h^2/2\pi m_x k_B T)^{1/2}$ is the thermal de Broglie wavelength (h is Planck's constant, m_x is the mass of species x, and k_B is the Boltzmann constant), V_x is the volume explored by species x, and $z_{\mathrm{int},x}$ is the contribution to the partition function due to all internal degrees of freedom. The hybridization free energy is given by

$$\Delta G_{AB} = -k_B T \ln\left(\frac{Z_{AB}}{Z_A Z_B}\right) \tag{3}$$

(11) SantaLucia, J. J. *Proc. Natl. Acad. Sci. U.S.A.* **1998**, *95*, 1460–1465.
(12) Maye, M. M.; Nykypanchuk, D.; van der Lelie, D.; Gang, O. *Small* **2007**, *3*, 1678–1682.
(13) Kim, A. J.; Biancaniello, P. L.; Crocker, J. C. *Langmuir* **2006**, *22*, 1991–2001.
(14) Xiong, H.; van der Lelie, D.; Gang, O. *Phys. Rev. Lett.* **2009**, *102*, 015504.
(15) Jin, R.; Wu, G.; Li, Z.; Mirkin, C. A.; Schatz, G. C. *J. Am. Chem. Soc.* **2003**, *125*, 1643–1654.
(16) Nykypanchuk, D.; Maye, M. M.; van der Lelie, D.; Gang, O. *Langmuir* **2007**, *23*, 6305–6314.
(17) Dreyfus, R.; Leunissen, M. E.; Sha, R.; Tkachenko, A. V.; Seeman, N. C.; Pine, D. J.; Chaikin, P. M. *Phys. Rev. Lett.* **2009**, *102*, 048301.
(18) Valignat, M. P.; Theodoly, O.; Crocker, J. C.; Russel, W. B.; Chaikin, P. M. *Proc. Natl. Acad. Sci. U.S.A.* **2005**, *102*, 4225–4229.
(19) Maye, M. M.; Nykypanchuk, D.; Van der Lelie, D.; Gang, O. *J. Am. Chem. Soc.* **2006**, *128*, 14020–14021.
(20) Geerts, N.; Schmatko, T.; Eiser, E. *Langmuir* **2008**, *24*, 5118–5123.
(21) Hill, H. D.; Macfarlane, R. J.; Senesi, A. J.; Lee, B.; Park, S. Y.; Mirkin, C. A. *Nano Lett.* **2008**, *8*, 2341–2344.
(22) Leunissen, M. E.; Dreyfus, R.; Cheong, F. C.; Grier, D. G.; Sha, R.; Seeman, N. C.; Chaikin, P. M. *Nat. Mater.* **2009**, *8*, 590–595.
(23) Russel, W.; Saville, D.; Schowalter, W. *Colloidal Dispersions*; Cambridge University Press: Cambridge, U.K., 1999.

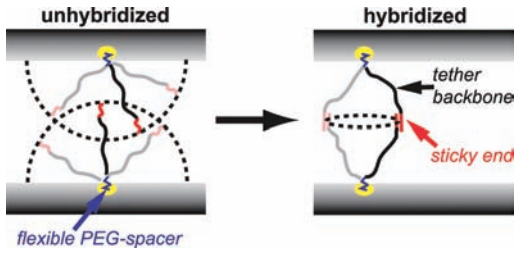

Figure 2. Configurational entropy cost. In the unhybridized state (left) the tethered sticky ends can explore space independently, whereas in the hybridized state (right) they are forced to move together. This restricted freedom of motion leads to an additional configurational entropy cost as compared to DNA in solution.

If we consider a single pair of sticky ends ($N_{AB} = N_A = N_B = 1$), then

$$\frac{Z_{AB}}{Z_A Z_B} = \frac{V_{AB}}{V_A V_B} \frac{z_{int,AB}/\Lambda_{AB}^{\ 3}}{z_{int,A} z_{int,B}/\Lambda_A^{\ 3}\Lambda_B^{\ 3}} \tag{4}$$

For sticky ends tethered to a surface, the hybridized AB product will explore a volume different from that which the unhybridized A and B sticky ends explore ($V_{AB} \neq V_{A,B}$), because after hybridization the two sticky ends have to move together while their surface attachment points are fixed (Figure 2). If we assume that $z_{int,x}$ does not change when the sticky ends are tethered to a surface, we can relate eqs 3 and 4 to the known equilibrium constant $K_{eq,AB} = \exp(-\Delta G^\circ_{AB,solution}/k_B T)$ for the hybridization of nontethered sticky ends in solution, for which $V_{AB} = V_A = V_B = V$. Using eq 2, the chemical potential $\mu = (\partial G/\partial N)_{P,T}$, the equilibrium condition $\mu_A + \mu_B = \mu_{AB}$, and the number density $\rho = N/V$, we find that

$$\frac{\rho_{AB}}{\rho_A \rho_B} = \frac{z_{int,AB}/\Lambda_{AB}^{\ 3}}{z_{int,A} z_{int,B}/\Lambda_A^{\ 3}\Lambda_B^{\ 3}} = \frac{K_{eq,AB}}{\rho^\circ} \tag{5}$$

with ρ° the standard number density (1 mol/L = 6. 022 $\times$ 10^{26} m^{-3}). Combination with eqs 3 and 4 finally gives an expression for the hybridization free energy of a pair of tethered sticky ends:

$$\begin{aligned} \Delta G_{AB,tether} &= -k_B T \ln\left(\frac{V_{AB}}{V_A V_B}\frac{K_{eq,AB}}{\rho^\circ}\right) \\ &= \Delta G^\circ_{AB,solution} - k_B T \ln\left(\frac{V_{AB}}{V_A V_B}\frac{1}{\rho^\circ}\right) \\ &= \Delta G^\circ_{AB,solution} - T\Delta S_{conf} \end{aligned} \tag{6}$$

The configurational entropy cost, ΔS_{conf}, that needs to be added to the hybridization free energy in solution can be estimated from geometric considerations[17] or, as we do here, obtained from fits to the experimental data. We point out that in general a sticky end can choose its binding partner from multiple complementary sticky ends that are within reach on the opposing particle surface. Each of the possible binding configurations will have a slightly different configurational entropy cost. Therefore, ΔS_{conf} in eq 6 should be considered an average value, while the effect of having several distinguishable bound configurations is taken into account in an approximate manner in eq 13 as the "binding multiplicity", m.

Association−Dissociation Kinetics of DNA-Functionalized Particles. For the sake of simplicity, we model the association and dissociation of DNA-functionalized particles with the reaction that interconverts singlets (S, concentration c_1) and doublets (S_2, concentration c_2). For self-complementary particles[24]

$$2S \underset{k_{off}}{\overset{k_{on}}{\rightleftharpoons}} S_2 \tag{7}$$

To calculate the flux of particles from one state to the other, we need expressions for the association and dissociation rate parameters, k_{on} and k_{off}. The association rate parameter is given by the diffusive flux of singlets and is in our essentially two-dimensional (2D) experiments[25] $k_{on} = 4\pi D$, with the diffusion constant $D = k_B T/6\pi\eta R_p$, where η is the suspending fluid viscosity and R_p the particle radius. The dissociation rate parameter follows from the relation

$$\frac{k_{on}}{k_{off}} = \frac{K_{eq,bead}}{c^\circ} \tag{8}$$

where $c^\circ = N^\circ/A$ is an arbitrary (2D) reference concentration (N° is the number of particles and A is the total system area). By considering the equilibrium condition $2\mu_S = \mu_{S_2}$ we find

$$\frac{K_{eq,bead}}{c^\circ} = \frac{\Lambda_S^{\ 2}}{\Lambda_{S_2}^{\ 2}} l^2 \exp\left(-\frac{\Delta F_{bead}}{k_B T}\right) = 2l^2 \exp\left(-\frac{\Delta F_{bead}}{k_B T}\right) \tag{9}$$

Here, ΔF_{bead} is the binding free energy of two DNA-functionalized particles (see the next section) and l is the distance along the interparticle bond over which a particle inside a doublet can move without losing the attractive interaction with the other particle.[26] We use $l = (l_{DNA} - d/2)/2$, where l_{DNA} is the length of the DNA construct and d is the equilibrium binding distance of the beads. To derive eq 9, we used the following expressions for the partition functions of, respectively, a 2D gas of singlets and a 2D gas of doublets of self-complementary particles:

$$\begin{aligned} Z_S &= \frac{1}{N_S!}\frac{A^{N_S}}{\Lambda_S^{\ 2N_S}} \\ Z_{S_2} &= \frac{1}{N_{S_2}!}\frac{A^{N_{S_2}}}{\Lambda_{S_2}^{\ 2N_{S_2}}}\left(\frac{l}{\Lambda_S}\right)^{2N_{S_2}} \exp\left(-\frac{\Delta F_{bead}}{k_B T}\right)^{N_{S_2}} \end{aligned} \tag{10}$$

Binding Free Energy of DNA-Functionalized Particles. Below we derive the bead−bead binding free energy, ΔF_{bead}, for the case where the sticky ends on the particles can form secondary structures. The example expressions given here apply to DNA constructs that can form intraparticle loops and two different kinds of hairpins, such as the single-stranded, self-complementary P_3 construct in Supporting Information Figure 1. Similar expressions can be derived in an entirely analogous way for systems with different secondary structures or for conventional, secondary-structure-free DNA-functionalized particles.

In our experiments, we first quench the system temperature, typically in a few minutes of time, and then ramp it slowly back up; see, for example, Figure 4. Importantly, the time scale of hybridization of our short DNA sticky ends is microseconds, whereas micrometer-sized particles diffuse on a time scale of

(24) Similar expressions apply to regular Watson−Crick pairs of complementary particles; these can be derived in an entirely analogous way.
(25) Smoluchowski, M. V. *Z. Phys. Chem.* **1917**, *92*, 129–168.
(26) Charbonneau, P.; Frenkel, D. *J. Chem. Phys.* **2007**, *126*, 196101.

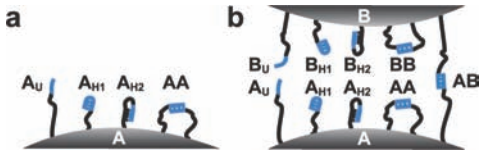

Figure 3. Nomenclature for the hybridization configurations of the P_3 construct: (a) on an isolated particle, (b) for two particles in prolonged contact.

seconds to minutes.[23] Consequently, by the time two particles encounter each other their individual DNA coatings will have reached a hybridization equilibrium with respect to secondary structure formation. Moreover, we find that at our experimental temperatures the conversion of loops and hairpins into interparticle bridges occurs on a time scale that is significantly longer than the duration of a diffusive particle encounter, which is estimated to last ~0.2 ms on average.[23] Therefore, we assume that in the early stages of particle association during the temperature quench ΔF_{bead} is determined by the fraction of "open", or "unprotected", sticky ends that are available for interparticle bridging at the moment of collision. This fraction follows from the partition function of all the different hybridization configurations[27] on an isolated particle (Figure 3a):

$$Z_{i,\mathrm{total}} = \sum_{N_A,N_{AA}} \frac{N_A^\circ!}{N_A!N_{AA}!} Z_A{}^{N_A} Z_{AA}{}^{N_{AA}} \tag{11}$$

with N_A° the total number of sticky ends, N_A the number of monomolecular structures A (which includes the unfolded structure, A_U, and the two hairpin structures, A_{H1} and A_{H2}), and N_{AA} the number of loops AA and with the partition functions

$$\begin{aligned} Z_A &= 1 + \exp\left(-\frac{\Delta G^\circ_{\mathrm{hairpin\,1}}}{k_BT}\right) + \exp\left(-\frac{\Delta G^\circ_{\mathrm{hairpin\,2}}}{k_BT}\right) \\ Z_{AA} &= \exp\left(-\frac{\Delta G_{\mathrm{loop}}}{k_BT}\right) \end{aligned} \tag{12}$$

We set the free energy of the unhybridized construct, ΔG°_{AU}, equal to zero and $\Delta G_{\mathrm{loop}} = \Delta G^\circ_{\mathrm{solution}} - T\Delta S_{\mathrm{conf,loop}}$ (eq 6). The number of loops runs from $N_{AA} = 0$ to $N_{AA} = N_{\mathrm{max}}/2$, and $N_A = N_{AH1} + N_{AH2} + N_{AU}$, with the number of hairpins running from $N_{AH1} = 0$ to $N_{AH1} = N_{\mathrm{max}} - 2N_{AA}$ and from $N_{AH2} = 0$ to $N_{AH2} = N_{\mathrm{max}} - 2N_{AA} - N_{AH1}$, while the number of unprotected sticky ends is $N_{AU} = N_{\mathrm{max}} - 2N_{AA} - N_{AH1} - N_{AH2}$. In principle, one has to take all the different realizations for each number of loops and hairpins explicitly into account while considering the specific positions of attachment of the sticky ends to the particle surface. We find, however, that for our experimental fits eq 11 is well-approximated by the much simpler expression for a "reactive mixture" of the different hybridized species in solution, Supporting Information eq 1. With a moderate correction of only ~5% (~0.5 k_BT) to $\Delta S_{\mathrm{conf,loop}}$ this expression predicts nearly the same bond distributions as the full expansion for all possible realizations. Supporting Information eq 1 assumes that each of the N_{max} sticky ends can bind to any of the $N_{\mathrm{max}} - 1$ other sticky ends. Therefore, to not overestimate the number of loops, we define an effective interaction patch on the particle surface inside which this is approximately true. If we assume that a sticky end can bind to any other sticky end within a radius of $2l_{\mathrm{DNA}}$, we obtain $N_{\mathrm{max,loop}} = (l_{\mathrm{DNA}}{}^2/R_p{}^2)N_{\mathrm{total}}$, with N_{total} the total number of sticky ends that is grafted to a particle. We model short double-stranded constructs as rigid rods with $l_{\mathrm{DNA}} = nl_{\mathrm{bp}}$, where n is the number of nucleotides in each of the DNA strands and $l_{\mathrm{bp}} = 0.34$ nm is the contribution of one base pair to the length of the double helix. Single-stranded constructs are modeled as a wormlike chain with an equilibrium end-to-end distance $(2bl_pn)^{1/2}$, with $b \approx 0.63$ nm the size of a nucleotide and $l_p \approx 2.7$ nm the persistence length at 50 mM NaCl.[28]

Equations 11 and 12 allow us to calculate the bond distributions on the individual particles as a function of the temperature using the predicted solution hybridization free energies (see the Experimental Section) and including an appropriate configurational entropy cost for the loops. Finally, we obtain ΔF_{bead} by inserting the fraction of unprotected sticky ends, f_{AU}, into the expression that we derived in ref 17 for two surfaces that interact with a certain fixed number of open sticky ends:

$$\Delta F_{\mathrm{bead}} = -k_BT \ln\left(\left[1 + f_{AU} m \exp\left(-\frac{\Delta G_{\mathrm{bridge}}}{k_BT}\right)\right]^{f_{AU}N_b} - 1\right) \tag{13}$$

Here, $N_b = \{[R_p(l_{\mathrm{DNA}} - d/2)]/[2(R_p + l_{\mathrm{DNA}})^2]\}N_{\mathrm{total}}$ is the maximum number of interparticle bridges that can form if all sticky ends on the beads are open, $m = [(l_{\mathrm{DNA}}{}^2 - d^2/4)/R_p{}^2]N_{\mathrm{total}}$ is the number of different complementary sticky ends on the opposing particle surface that a particular sticky end can choose to bind to, and $\Delta G_{\mathrm{bridge}} = \Delta G^\circ_{\mathrm{solution}} - T\Delta S_{\mathrm{conf,bridge}}$ (eq 6).

To model the particles' dissociation transition when we ramp the temperature back up, we follow a similar approach, but now we consider the equilibrium that includes intra- and interparticle hybridization simultaneously, because the particles inside the aggregates are in prolonged contact before they dissociate, allowing for the interconversion of loops, hairpins, and interparticle bridges. The total partition function for two particles (A and B) in contact is (Figure 3b)

$$Z_{c,\mathrm{total}} = \sum_{N_A,N_B,N_{AA},N_{BB},N_{AB}} \frac{N_A^\circ!N_B^\circ!}{N_A!N_B!N_{AA}!N_{BB}!N_{AB}!} \times Z_A{}^{N_A} Z_B{}^{N_B} Z_{AA}{}^{N_{AA}} Z_{BB}{}^{N_{BB}} Z_{AB}{}^{N_{AB}} \tag{14}$$

where N_{AB} is the number of interparticle bridges and all other N_x are analogous to the isolated particle case described above. Further, $N_{AB} = 0$ to N_{max}, $N_{AA/BB} = 0$ to $(N_{\mathrm{max}} - N_{AB})/2$, $N_{AH1/BH1} = 0$ to $N_{\mathrm{max}} - N_{AB} - 2N_{AA/BB}$, $N_{AH2/BH2} = 0$ to $N_{\mathrm{max}} - N_{AB} - 2N_{AA/BB} - N_{AH1/BH1}$, and $N_{AU/BU} = N_{\mathrm{max}} - N_{AB} - 2N_{AA/BB} - N_{AH1/BH1} - N_{AH2/BH2}$. For the self-complementary P_3 sticky ends

$$\begin{aligned} Z_A = Z_B &= 1 + \exp\left(-\frac{\Delta G^\circ_{\mathrm{hairpin\,1}}}{k_BT}\right) + \exp\left(-\frac{\Delta G^\circ_{\mathrm{hairpin\,2}}}{k_BT}\right) \\ Z_{AA} = Z_{BB} &= \exp\left(-\frac{\Delta G_{\mathrm{loop}}}{k_BT}\right) \\ Z_{AB} &= \exp\left(-\frac{\Delta G_{\mathrm{bridge}}}{k_BT}\right) \end{aligned} \tag{15}$$

Similar to the isolated particle case, we can approximate eq 14 with the reactive mixture expression of Supporting Information eq 2, while N_{max} follows from the average of the effective

(27) Dimitrov, R. A.; Zuker, M. *Biophys. J.* **2004**, *87*, 215–226.

(28) Murphy, M. C.; Rasnik, I.; Cheng, W.; Lohman, T. M.; Ha, T. *Biophys. J.* **2004**, *86*, 2530–2537.

interaction patches for loop formation (given below eq 12) and for interparticle bridge formation. The latter gives $N_{max,bridge} = [(l_{DNA}^2 - d^2/4)/R_p^2]N_{total}$ as the number of sticky ends on the opposing particle surface that a sticky end can geometrically bind to. We obtain the best fits to our experimental data when we set the binding distance of the beads, d, equal to $1.5l_{DNA}$ for double-stranded constructs and to the equilibrium end-to-end distance of a wormlike chain of $2n$ nucleotides for single-stranded constructs. The binding free energy for two beads that interact through a patch of N_{max} sticky ends on each of their surfaces then is

$$\Delta F_{patch} = -k_B T[\ln(Z_{c,bound}) - \ln(Z_{c,unbound})] \qquad (16)$$

Here, $Z_{c,bound} = Z_{c,total} - Z_{c,unbound}$, and $Z_{c,unbound}$ is the partition function of all the states in which the particles are not bound, i.e., $N_{AB} = 0$ (Supporting Information eq 3). In reality, the contact area between two beads contains $N_b = \{[R_p(l_{DNA} - d/2)]/[2(R_p + l_{DNA})^2]\}N_{total}$ sticky ends that can participate in binding, giving the following approximate total bead−bead binding free energy:

$$\Delta F_{bead} = \frac{N_b}{N_{max}}\Delta F_{patch} \qquad (17)$$

Fitting the Experimental Data. In the experimental temperature cycles, each time t corresponds to a particular temperature, $T(t)$. Consequently, ΔF_{bead} (eqs 13 and 17) and the association and dissociation rate parameters, k_{on} and k_{off} (eq 8), are effectively time dependent. Using the experimental temperature profiles and the singlet concentration c_1 at $t = 0$ as input, we fit the experimental data by numerically solving for the evolution of the rate equations that govern the particles' association−dissociation reaction in eq 7:

$$\begin{cases} \dfrac{dc_1}{dt} = -2k_{on}(t)\, c_1(t)^2 + 2k_{off}(t)\, c_2^*(t) \\ \dfrac{dc_2}{dt} = k_{on}(t)\, c_1(t)^2 - k_{off}(t)\, c_2^*(t) \end{cases} \qquad (18)$$

We model the dissociation transition of the aggregates, which occurs when the temperature is ramped back up in the second part of the experiment, by using the conventional expression $c_2^*(t) = c_2(t)$ and taking eq 17 for ΔF_{bead}. For the aggregation process during the temperature quench in the first part of the experiment we use eqs 11−13, but now we have to take into account that any doublets formed at the higher temperature $T(t_1)$ will later have a much smaller dissociation rate at the lower temperature $T(t_2)$. Namely, the number of bridges between the particles in the doublet remains the same (or even increases due to loop and hairpin opening), while ΔG_{bridge} in eq 13 decreases linearly with the temperature, becoming more negative. In principle, however, our simple model does not distinguish between previously (at $T(t_1)$) and newly (at $T(t_2)$) formed doublets: when integrating the rate equations, all doublets are heaped together inside a single concentration c_2 and are assigned a dissociation rate that is based on the ΔF_{bead} value from eq 13 that corresponds to the current temperature $T(t)$. At lower temperature there will be more secondary structure formation and thus fewer interparticle bridges, meaning that at $T(t_2)$ eqs 11−13 would predict a too high dissociation rate for the population of doublets that formed earlier at $T(t_1)$ with more interparticle bridges. Therefore, during the temperature quench we limit the dissociation to recently formed doublets, within the preceding τ seconds, and set $c_2^*(t) = c_2(t) - c_2(t-\tau)$, effectively taking the population of "old", strongly bound doublets out of the equation. For τ we use a value that experimentally corresponds to a change of ~1 °C in the temperature profile—the typical width of our particles' dissociation transition. We point out, however, that the results are not so sensitive to the exact choice of τ within the range of reasonable values. Finally, for the most accurate results we fit the association and dissociation curves simultaneously using the configurational entropy costs of the loops and bridges as the only free parameters; all other parameters are kept fixed at their known or estimated values.

Results and Discussion

Tether Backbones. When functionalizing particles with DNA, one of the first choices is whether to use single-stranded or double-stranded DNA for the backbone that tethers the sticky ends to the particle surface (Figure 2 and Supporting Information Figure 1). Although one might expect that a rigid double-stranded backbone (persistence length $l_p \approx 45-50$ nm)[29] does better at projecting the sticky ends away from the particle surface than a much more flexible single-stranded backbone ($l_p \approx 2.7$ nm at 50 mM NaCl),[28] possibly allowing for more interparticle bonds,[19] the effect of the backbone choice on the particles' association−dissociation behavior is not immediately clear. This is because the character of the backbone affects more than just the maximum number of interparticle bridges that can be formed (N_b) or the number of different complementary sticky ends on the opposing particle surface that a particular sticky end can choose to bind to (the binding multiplicity, m). The length and flexibility of the backbone are also major determinants of the configurational entropy cost that is associated with the hybridization of tethered DNA (Figure 2), thus affecting the overall bead−bead binding free energy, ΔF_{bead} (see e.g. eq 13), through the adjusted hybridization free energy of the tethered sticky end pairs (eq 6).

Figure 4 provides a simple illustration of the effect that the tether backbone can have on the particles' association−dissociation behavior. Here, we compare beads with exactly the same sticky ends, but in Figure 4a they are tethered to the surface through a single-stranded (SS) backbone and in Figure 4b through a double-stranded (DS) backbone. The number of nucleotides in the backbone strands is the same, but due to their different flexibilities the estimated end-to-end distance of the constructs is, respectively, $l_{DNA,SS} \approx 14$ nm and $l_{DNA,DS} \approx 23$ nm (see also below eq 12). In both cases, the C_N and C_N' sticky ends form a conventional Watson−Crick pair between complementary beads, Supporting Information Figure 1. By tracking the fraction of nonassociated "singlet" particles, while quenching the temperature (from 52 to 20 °C) and then ramping it back up, we reveal the characteristic association and dissociation behavior of the beads. Throughout this paper, we will apply this method, in conjunction with the theoretical model of the previous section, as an easy-to-use diagnostic tool that characterizes the effects of different DNA coatings.

In Figure 4, both the SS and DS beads display the typical behavior of conventional DNA-functionalized systems: when we drop below the particles' dissociation temperature (T_{dis}), the beads quickly come together in extensive structures and the singlet fraction decreases to zero; when we raise the temperature

(29) Taylor, W. H.; Hagerman, P. J. *J. Mol. Biol.* **1990**, *212*, 363–376.

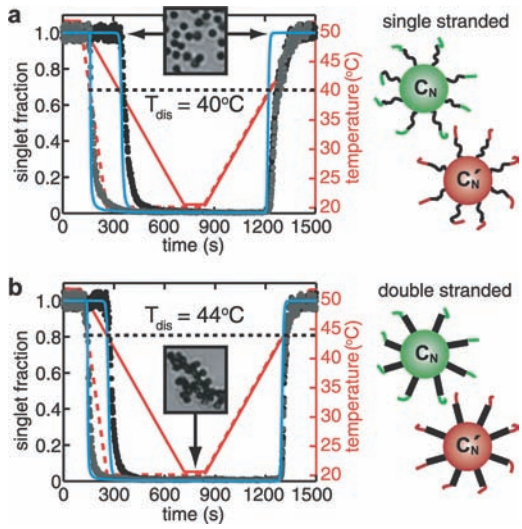

Figure 4. Association−dissociation behavior for conventional sticky ends with different tether backbones: (a) single-stranded backbone, (b) double-stranded backbone. Shown are the temperature (in red) and the corresponding particle singlet fraction (symbols) as a function of the elapsed time for two different quench rates. The solid red line and black dots correspond to the slowest temperature quench and the dashed red line and gray dots to the fastest quench. The blue lines are fits from our theoretical model. The microscopy insets show a small part of the sample in the fully dissociated state (a) and the fully associated state (b).

above T_{dis}, the aggregates quickly dissociate again. Here, we have defined T_{dis} as the temperature in the up-ramp at which the dissociation of the aggregates is seen to start, as reflected by an increase in the measured singlet fraction. Due to the sharp association−dissociation transition of the beads T_{dis} is nearly the same as the temperature at which association is seen to start during the initial quench, and therefore, we use just T_{dis} to characterize the system. In Figure 4, one can also see that the rate of temperature change only determines how fast T_{dis} is reached, but that it does not change the qualitative shape of the association and dissociation curves. These observations are in excellent agreement with the curves that follow from our theoretical model. Note, however, that especially in Figure 4a the experimentally observed dissociation of the aggregates ($t >$ 1200 s) is slower than predicted. We occasionally see this, but so far we have not found a clear correlation with the character of the DNA construct. The slight deviation from the predicted curves near the end of the aggregation process in the initial temperature quench is likely due to the slower dynamics of larger clusters, which is not accounted for by our model.

Despite their identical sticky ends, the dissociation temperature for the SS beads is about 4 °C lower than for the DS beads ($T_{dis,SS} \approx 40$ °C and $T_{dis,DS} \approx 44$ °C). Our theoretical model suggests that the reason for this difference is both a somewhat smaller number of SS interparticle bridges ($N_{b,SS} \approx 66$ versus $N_{b,DS} \approx 78$) and a larger configurational entropy cost for the hybridization of the single-stranded construct, $\Delta S_{conf,SS} = -15.6\ k_B$ and $\Delta S_{conf,DS} = -14.7\ k_B$. We point out that these values are in rough agreement with simple geometrical estimates.[17] However, it is difficult to predict them exactly a priori, because they depend not only on the flexibility of the tether backbone, but also on the grafting details, such as the method of attachment to the particle surface. Nevertheless, in ref 17 we have shown that, once the relevant configurational entropy cost for a particular DNA construct has been found by fitting a limited set of experimental data, it accurately predicts the association−dissociation properties of similar systems.

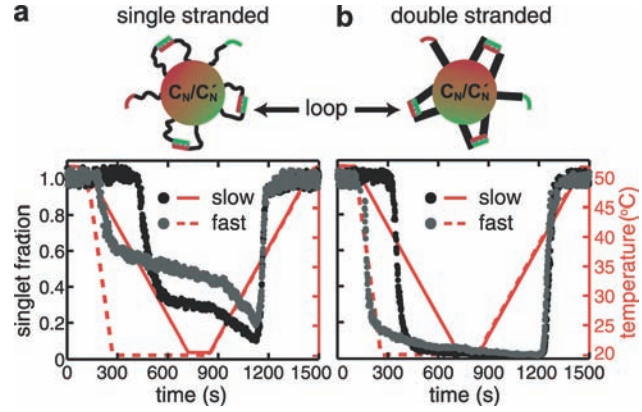

Figure 5. Association−dissociation behavior for conventional sticky ends mixed on the same bead: (a) single-stranded backbone, (b) double-stranded backbone. Shown are the temperature (in red) and the corresponding particle singlet fraction (symbols) as a function of the elapsed time for two different quench rates.

Intraparticle Loop Formation. For certain assembly schemes it can be advantageous to functionalize particles with self-complementary palindromic sticky ends instead of conventional Watson−Crick pairs (see, for example, the "self-replication" scheme in ref 30). With self-complementary sticky ends one needs to synthesize only one type of DNA construct and prepare only one type of particle, as the beads now have self-recognition capabilities. Obviously, this also means that the coordination of the particles in the associated state will likely be different, enabling new structures. The functionalization with self-complementary sticky ends comes with its own subtleties though, the most important of which is the possibility of hybridization between neighboring sticky ends on the same particle, here referred to as "loop formation". To unambiguously show that loop formation indeed occurs and to clearly demonstrate its impact on the particles' association−dissociation behavior, we first present in Figure 5 the effect of mixing the conventional C_N and C_N' sticky ends on the same bead, as these results can be directly compared to those in Figure 4. In Figure 5, the particle association initially starts off normally, but especially in the single-stranded backbone case of Figure 5a it later slows sharply. Apparently, at the start of the temperature quench interparticle bridges dominate, whereas at lower temperatures intraparticle loops dramatically reduce the number of open sticky ends that are available for bridge formation. The faster the quench, the higher the singlet fraction at which the association slows and the more pronounced the deviation from the association curves of the conventional systems in Figure 4. This is because in a faster quench there are fewer diffusive particle encounters before their interactions are completely inhibited by loop formation. In Figure 5a, one can also see that when the temperature is raised again, dehybridization of the loops reactivates the particle association, leading to a further dip in the singlet fraction before the beads enter the dissociation transition around $t = 1200$ s.

The hybridizing sequence is identical for the interparticle bridges and the intraparticle loops, and therefore, the suspension behavior depends sensitively on the respective configurational entropy costs. Again, it is difficult to predict these costs, but in a series of experiments with different sticky ends we reproducibly find that the configurational entropy cost of the loops is

(30) Leunissen, M. E.; Dreyfus, R.; Sha, R.; Wang, T.; Seeman, N. C.; Pine, D. J.; Chaikin, P. M. *Soft Matter* **2009**, *5*, 2422–2430.

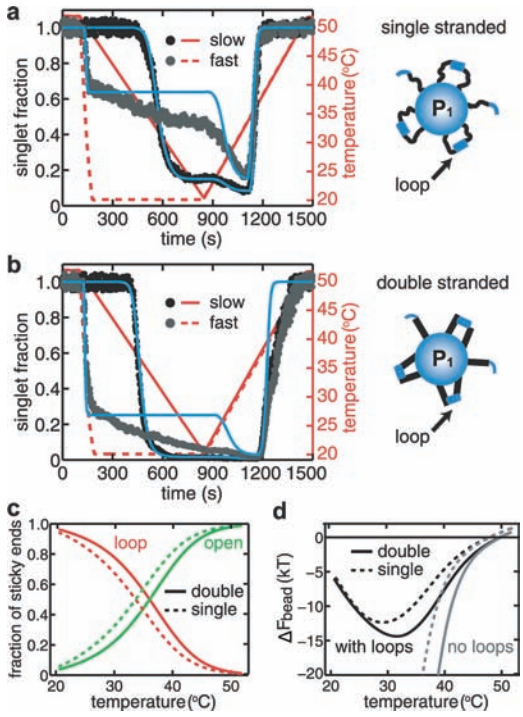

Figure 6. Experiment with the loop-forming self-complementary sequence P_1 for different tether backbones. (a, b) Graphs of the association−dissociation behavior with (a) a single-stranded backbone or (b) a double-stranded backbone. (c) Calculated relative bond distributions on an isolated bead as a function of the temperature for the single- and double-stranded constructs (from eq 11). (d) Calculated bead−bead binding free energy during the early stages of association as a function of the temperature (eq 13). For comparison, ΔF_{bead} is also shown for the hypothetical case in which the sticky ends cannot form any intrabead loops (i.e., all sticky ends are open at all temperatures).

slightly larger than that of the bridges, leading to behavior as observed in Figure 5 (both for single-stranded and double-stranded constructs). To obtain more quantitative insight, we performed a similar experiment with self-complementary sticky ends (P_1 in Supporting Information Figure 1), as this prevents experimental errors in the complementary sticky end ratio on the beads. We designed this palindromic sequence such that possible hairpin structures have a very low melting temperature and do not form under our experimental conditions. The association−dissociation behavior of the beads is shown in Figure 6a,b, and from our model we find $\Delta S_{bridge,SS} = -14.8\ k_B$ and $\Delta S_{loop,SS} = -15.2 \pm 0.2\ k_B$ for the construct with a single-stranded backbone and $\Delta S_{bridge,DS} = -13.9\ k_B$ and $\Delta S_{loop,DS} = -14.4 \pm 0.2\ k_B$ for the double-stranded construct. The fact that the ΔS_{loop} value varies a little for the same system at different quench rates may be an experimental artifact (i.e., uncertainty in the temperature readout) or may be due to an as yet unidentified dynamical effect in the DNA coating that is not accounted for by our model. Here, we arbitrarily choose to keep ΔS_{bridge} constant and to absorb any uncertainty in ΔS_{loop}. Although we can fit the dissociation transition around $t = 1200$ s and the point at which the initial association slows quite well, in the fast temperature quenches the experimental curves display a clear deviation from the predicted horizontal plateaus, which would correspond to a complete arrest of the association process. This deviation is caused by a "pairing problem" inside the DNA coatings of the individual beads which is not included in our model. Namely, there is always a certain fraction of sticky ends that fail to find a partner for loop formation and that thus remain available for interparticle bridge formation. We roughly estimate this fraction to be 0.15 using a two-dimensional mean-field approximation where each sticky end is surrounded by 12 other sticky ends that reside within a radius of $2l_{DNA}$ (for the typical surface coverage used in our experiments).

The difference between the bridge and loop configurational entropy costs is nearly the same in the single-stranded and double-stranded systems (∼0.4−0.5 k_B), leading to fairly similar bond distributions, Figure 6c. Nevertheless, the association−dissociation behavior of the DS particles (Figure 6b) is much less affected by the loop formation. This is likely due to the fact that in the DS system the individual interparticle bridges are somewhat stronger ($|\Delta S_{bridge,DS}| < |\Delta S_{bridge,SS}|$) and that the maximum number of bridges ($N_{b,DS} = 75$ versus $N_{b,SS} = 63$) and their binding multiplicity ($m_{DS} = 12$ versus $m_{SS} = 6$) are larger. All of these factors lead to a more negative bead−bead binding free energy (eq 13, Figure 6d) and thereby to a smaller dissociation rate parameter (k_{off} in eq 8) and a larger net particle association before the sticky ends are passivated at low temperature inside loops. Note that in Figure 6d the minimum in ΔF_{bead} as a function of the temperature is the result of a trade-off between a more negative bridge hybridization free energy at lower temperature and a decreasing number of interparticle bridges due to loop formation (compare with the curves for the case of no loop formation).

Hairpin Formation. From the previous section it is clear that intraparticle loop formation can have a large impact on the particles' binding strength and association kinetics. It actually forms a good basis for the creation of switchable self-protected interactions (see the Introduction and ref 22), provided that one can circumvent the aforementioned pairing problem. To this end we design the DNA constructs such that they can form not only loops, but also internally folded hairpin structures which involve the sticky end sequence. As a general example of the different hairpin possibilities, we study in Figure 7 two single-stranded DNA constructs (P_2 and P_3 in Supporting Information Figure 1) whose sticky end can form a single kind of hairpin with itself (Figure 7a) or one hairpin with itself and another kind of hairpin with the tether backbone (Figure 7b). All of these hairpin structures have a melting temperature of ∼34 °C.

If we compare the association−dissociation behavior of Figure 7 with that shown in Figure 6a (no hairpins), it is immediately clear that on the time scale of these experiments the introduction of hairpins indeed leads to the desired complete arrest of the association, as reflected by the nicely horizontal plateaus for $t \lesssim 900$ s. The calculated bond distributions in Figure 7c−f (corresponding to the fits in Figure 7a with $\Delta S_{bridge} = -13.4\ k_B$ and $\Delta S_{loop} = -14.2 \pm 0.2\ k_B$ and in Figure 7b with $\Delta S_{bridge} = -12.6\ k_B$ and $\Delta S_{loop} = -13.4 \pm 0.2\ k_B$) indicate that for both the P_2 and P_3 systems the main contribution to the self-protection comes from loop formation. The hairpins are important in circumventing the pairing problem though, because their monomolecular character enables them to protect any sticky ends that accidentally remain without a binding partner. This general role is also apparent from the more qualitative experiment in Figure 8, where we tried to keep a suspension of chainlike structures (Figure 8a) stable for a prolonged time. As expected, at high temperature the sticky ends are largely unprotected and the chains aggregate, Figure 8b. At low temperature, the P_3 sticky ends are well-protected by a combination of loops and hairpins and the suspension is entirely stable (Figure 8c). In contrast with this, chains that are functionalized with a construct that can only form loops (here P_1) suffer from

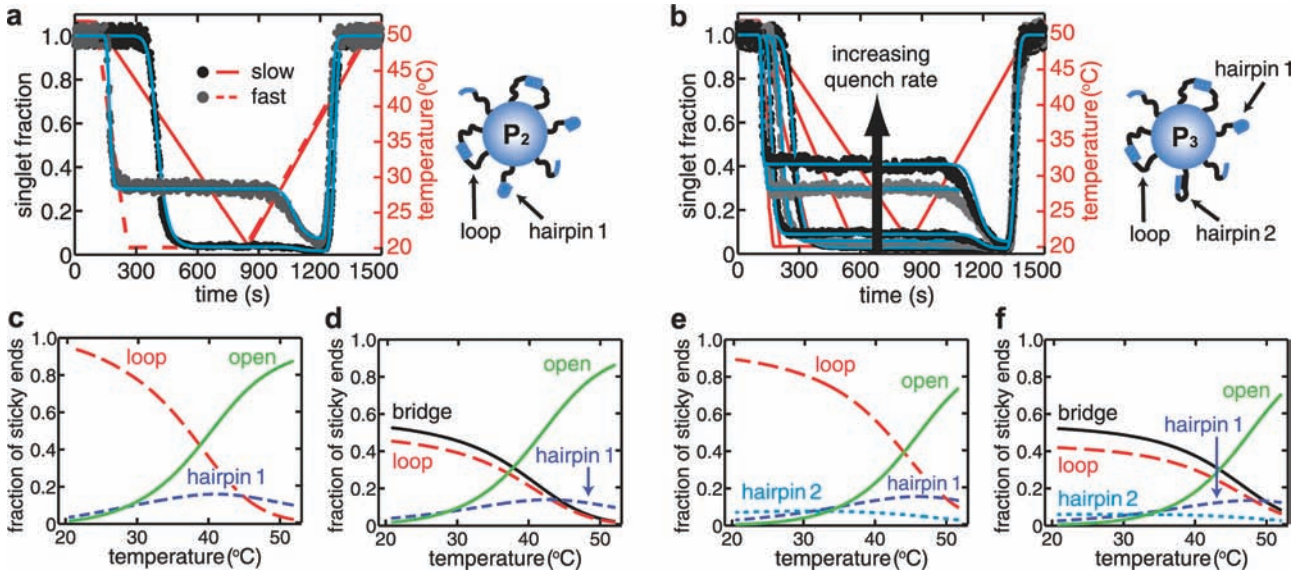

Figure 7. Experiment with the loop- and hairpin-forming self-complementary sequences P_2 and P_3. (a, b) Shown are the association−dissociation kinetics of (a) the P_2 construct, which can form one kind of hairpin, and (b) the P_3 construct, which can form two different hairpins. Both constructs have a single-stranded backbone. The curves are alternatingly colored black and gray for increasing quench rate; the blue lines are fits from our model. (c, d) Calculated relative bond distributions for (c) an isolated P_2 bead (from eq 11) or (d) the interaction area between two P_2 beads in prolonged contact (from eq 14). (e, f) Similar to (c) and (d), but for P_3 beads.

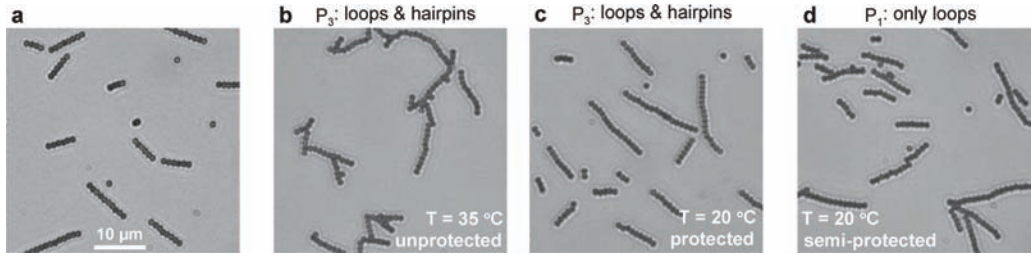

Figure 8. Self-protected interactions based on loop and hairpin formation. Using an external magnetic field, we brought the DNA-functionalized particles together inside linear chains, after which we lowered the temperature below the beads' dissociation temperature, followed by turning off the field. (a) shows a representative example of the resulting chain structures (note that, despite possible secondary structure formation, interparticle bridges form readily because the particles are held in close contact while the temperature is being lowered). (b−d) Chains after 60 min at the specified temperature for particles functionalized with (b, c) the loop- and hairpin-forming single-stranded P_3 sequence or (d) the single-stranded P_1 sequence, which can only form loops. The degree of aggregation of the P_1-functionalized chains is intermediate compared to the aggregation of the unprotected and protected P_3 chains.

the pairing problem, are less well-protected, and display some aggregation even at low temperature (Figure 8d).

The similarity of the curves in Figure 7a,b suggests that the effectiveness of the additional monomolecular protection does not depend on the number of different hairpins that can be formed. Consequently, we expect self-protection properties for the P_2 system similarly as good as those demonstrated for the P_3 system.[22] Figure 9 provides a convenient representation of the temperature-dependent attenuation of the aggregation rate that was achieved for P_3-functionalized particles, as compared to regular sticky spheres that display diffusion-limited aggregation. For ease of use, the experimental temperature is here expressed relative to the melting temperature, $T_{m,solution}$, that a pair of sticky ends would have if they were free in solution at a concentration similar to that in the DNA coating on the beads (estimated to be ~0.5 mM). We chose this particular temperature as a reference, because we have shown that in the P_3 system hybridization of the sticky ends inside loops accounts for most of the self-protection effect, because this temperature is readily obtainable from the Mfold Web server[31] (obviating the need to experimentally determine another characteristic temperature for

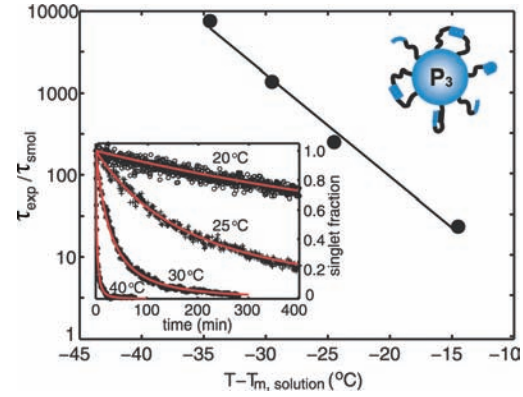

Figure 9. Temperature dependence of the P_3-mediated self-protection. The characteristic aggregation time, τ_{exp}, for P_3-functionalized beads is scaled by the Smoluchowski time for diffusion-limited aggregation, $\tau_{smol} = 1/(2\pi D c_{bead})$, and plotted as a function of the difference between the (fixed) experimental temperature and the predicted melting temperature of the P_3 sticky ends in solution, $T_{m,solution} \approx 54.5$ °C. The inset shows the experimental aggregation curves at the different temperatures (symbols) and the corresponding fits to the Smoluchowski aggregation equation (in red), $f_{singlet}(t) = (1 + t/\tau_{exp})^{-2}$.

(31) Zuker, M. *Nucleic Acids Res.* **2003**, *31*, 3406–3415.

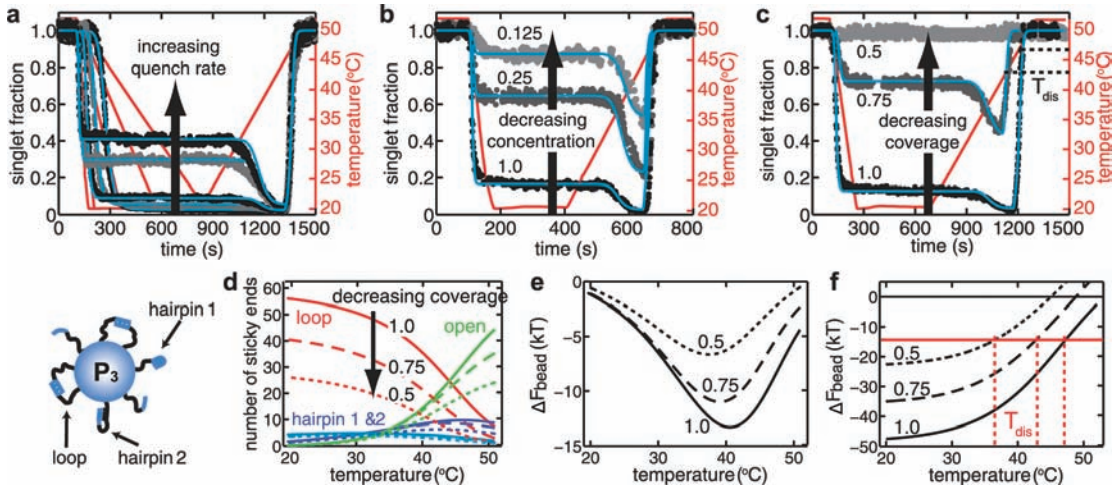

Figure 10. Behavior of the single-stranded P_3 construct under a range of conditions. (a−c) Shown are the association−dissociation kinetics as a function of (a) the quench rate, (b) the particle concentration ($c_{bead} = 1.0$ corresponds to $\sim 2.8 \times 10^{11}$ particles/m^2), and (c) the sticky end coverage on the beads ($\sigma = 1.0$ corresponds to 15 500 sticky ends/particle); the blue lines are theoretical fits. For the different sticky end coverages we have plotted (d) the calculated bond numbers in the interaction area of a single bead (from eq 11; the smaller the coverage, the finer the dash), (e) the bead−bead binding free energy during the early stages of association (eq 13), and (f) the binding free energy for beads that are in prolonged contact (eq 17). The solid red line in (f) connects the points on the free energy curves that correspond to the dissociation temperatures observed in (c).

the system) and because one can expect different DNA constructs with a similar backbone and a similar $T_{m,solution}$ for their sticky ends to give rise to a similar attenuation of the aggregation rate. One can see that for temperatures 15−35 °C below $T_{m,solution}$ the aggregation slows by a rapidly increasing factor of 20×−10000×. This strong temperature response is a result of the temperature dependence of the fraction of unprotected sticky ends (Figure 7e) and can be used to repeatedly activate and deactivate the particle association (e.g., Figure 1).

General Factors: Quench Rate, Particle Concentration, and Surface Coverage. To facilitate comparison, we reproduce in Figure 10a the series of measurements for the P_3 construct at different temperature quench rates, which was shown earlier in Figure 7b. Together with the series of experiments at a fixed quench rate but different particle concentrations, Figure 10b, these measurements illustrate nicely how the overall association behavior of systems with secondary structure formation is determined by a competition between the quench rate and the particles' diffusive encounter rate. The faster the quench or the lower the bead concentration, the fewer the associative particle collisions that occur before the sticky ends are passivated inside secondary structures, and the higher the singlet fraction at which the association arrests. Importantly, all of the curves can be fit with $\Delta S_{bridge} = -12.6\ k_B$ and $\Delta S_{loop} = -13.4 \pm 0.2\ k_B$, and in all cases $T_{dis} \approx 47$ °C. This is only true, however, if we keep the density of the sticky end coverage on the particle surface constant, i.e., if we use a fixed number of sticky ends per bead.

In Figure 10c we systematically changed the sticky end coverage by dilution with nonsticky $(dT)_{11}$ ends and studied its effect on the association−dissociation behavior. It can be seen that in our quench experiments a change from 100% to 75% sticky ends already gives rise to a tremendous reduction of the particle association, while for 50% sticky ends no association occurs at all. As expected, the reduction in the sticky end coverage also shifts the dissociation temperature down ($T_{dis,100\%} \approx 47$ °C and $T_{dis,75\%} \approx 43$ °C) as the maximum number of interparticle bridges decreases from $N_{b,100\%} = 63$ to $N_{b,75\%} = 47$ and $N_{b,50\%} = 31$ if all sticky ends are open. In addition to this, from our theoretical fits we find a small increase in the absolute configurational entropy costs for bridge and loop formation when the coverage is reduced: $\Delta S_{bridge,100\%} = -12.6\ k_B$, $\Delta S_{loop,100\%} = -13.5\ k_B$ and $\Delta S_{bridge,75\%} = -12.7\ k_B$, $\Delta S_{loop,75\%} = -13.7\ k_B$. At present, this finding is based on a still somewhat limited experimental data set, but from a purely geometrical point of view it seems likely that bond formation is more costly at lower coverage, because in that case the DNA constructs on average have to stretch out further to find a binding partner. Extrapolating the trend in the ΔS_{conf} values, we estimate for 50% sticky ends that $T_{dis,50\%} \approx 37$ °C; it further is predicted that for the temperature profile of Figure 10c no significant particle association occurs, in agreement with the experimental observations.

We point out that the main factor in the coverage dependence of the association−dissociation behavior is the change in the number of bridges, $f_{AU}N_b$ in eq 13, that can form between two particles if one takes the secondary structure formation into account (f_{AU} is the fraction of open sticky ends). For the early stages of association we find the bond numbers shown in Figure 10d. From this graph one can see that at lower coverage hairpin formation becomes somewhat more important relative to loop formation. Overall, however, the relative distribution of the bonds does not change much. Thus, the less negative bead−bead binding free energy at lower coverage (Figure 10e) must be a direct consequence of the reduction in the absolute number of bonds and not a changing bond distribution. Note that in our model the temperature-dependent bead−bead binding free energy is different during the initial stages of association in the temperature quench (Figure 10e) and during the final dissociation of the aggregates (Figure 10f), around $t = 1100-1200$ s in the temperature ramp of Figure 10c. The reason is that it takes some time for the loops and hairpins to open up and to form more stable interparticle bridges; see also the discussion before eq 11. If we superpose the dissociation temperatures observed in Figure 10c onto the free energy curves in Figure 10f, we find that at the experimental particle concentration dissociation occurs when $\Delta F_{bead} \gtrsim -14\ k_BT$.

We performed a similar series of experiments as a function of the temperature quench rate, the particle concentration, and the surface coverage for the same P_3 sticky ends attached to a double-stranded tether backbone, Figure 11. In this case, the

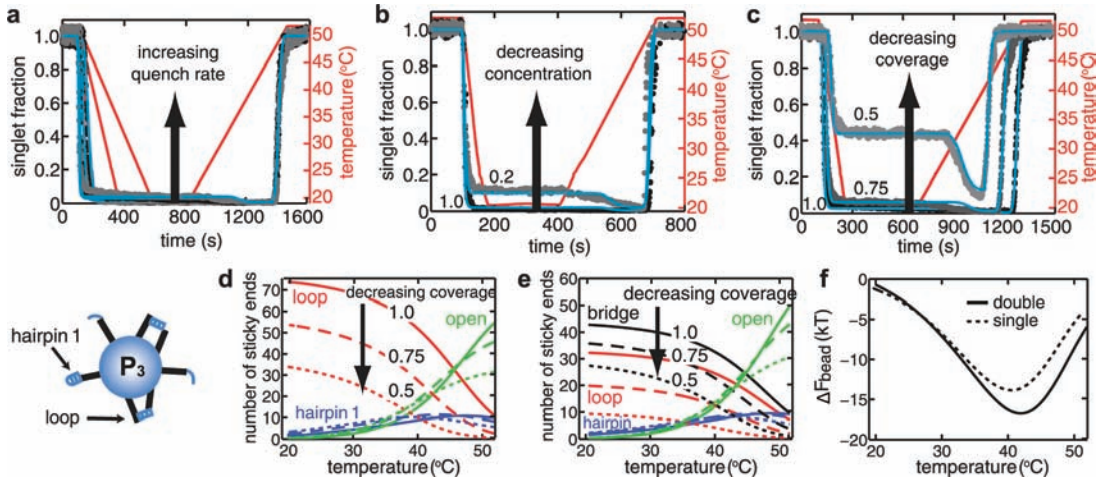

Figure 11. Behavior of the double-stranded P_3 construct under a range of conditions. (a−c) Shown are the association−dissociation kinetics as a function of (a) the quench rate, (b) the particle concentration ($c_{bead} = 1.0$ corresponds to $\sim 1.6 \times 10^{11}$ particles/m^2), and (c) the sticky end coverage on the beads ($\sigma = 1.0$ corresponds to 15 500 sticky ends/particle); the blue lines are theoretical fits. (d, e) Absolute bond numbers in (d) the interaction area of a single bead and (e) the interaction area between two beads in prolonged contact, calculated for different sticky end coverages (the smaller the coverage, the finer the dash). (f) Comparison of the bead−bead binding free energy during the early stages of association for the double-stranded and single-stranded (from Figure 10) P_3 construct ($\sigma = 1.0$).

sticky ends can form loops and their own hairpins, but no secondary structures that involve the backbone sequence (Supporting Information Figure 1). After our studies on the single-stranded P_2/P_3 constructs (Figures 7 and 10) and the double-stranded P_1 construct (Figure 6) the observed behavior for the double-stranded P_3 construct is largely as expected. For instance, we again find that for a constant surface coverage (100%) we can fit all of the curves at different quench rates (Figure 11a) and particle concentrations (Figure 11b) with a single set of configurational entropy costs: $\Delta S_{bridge,100\%} = -12.9\ k_B$ and $\Delta S_{loop,100\%} = -13.8\ k_B$. The somewhat more limited configurational flexibility of the rigid double-stranded construct could possibly explain the slightly stronger dependence of the configurational entropy costs and of the bond distributions on the surface coverage, as compared to the single-stranded P_3 construct. In Figure 11c $\Delta S_{bridge,100\%} = -12.9\ k_B$ and $\Delta S_{loop,100\%} = -13.8\ k_B$, $\Delta S_{bridge,75\%} = -13.6\ k_B$ and $\Delta S_{loop,75\%} = -14.8\ k_B$, and $\Delta S_{bridge,50\%} = -14.0\ k_B$ and $\Delta S_{loop,50\%} = -15.7\ k_B$, giving the calculated bond distributions of Figure 11d,e. At reduced coverage, the larger difference between the ΔS_{bridge} and ΔS_{loop} values increases the relative importance of interparticle bridge formation over intraparticle loop formation (Figure 11e). Apparently, the loops are somewhat more sensitive to the average spacing between the surface attachment points of the sticky ends. This could have to do with the fact that they consist of sticky ends on the same bead, instead of overlapping sticky ends from opposing particle surfaces. Similar to the situation in Figure 6, we see that the double-stranded tether backbone again suppresses the effect of secondary structure formation on the particles' association behavior (compare, for instance, Figure 11a and Figure 10a) due to an overall more negative bead−bead binding free energy, Figure 11f. It is important to note, however, that the apparent absence of such an effect under certain conditions (e.g., the experiment in Figure 11a) does not mean that it cannot be a major factor under other conditions. This is best illustrated by the experiments in Figure 11c and, to a lesser extent, Figure 11b. Clearly, if we slow the association by lowering the particle concentration or by reducing the sticky end coverage, loop and hairpin formation play a more pronounced role, as signified by the horizontal plateau and subsequent dip that develop in the association−dissociation curves and that are characteristic of the competition between intraparticle and interparticle hybridization.

Conclusions

We have shown that a straightforward measurement of the particles' association−dissociation kinetics during selected temperature cycles can give valuable insight into the structural and dynamical properties of their DNA coatings, including possible secondary structure formation. It also forms a sensitive test for kinetic effects that can occur under the conditions of interest, but that could go unnoticed in a measurement at fixed temperature. We find that for identical sticky ends the character of the tether backbone can have a significant effect on the particles' dissociation temperature, both through the number of interparticle bridges that are formed and through their configurational entropy cost. Our experiments also show that secondary structure formation becomes increasingly important in faster temperature quenches, at lower particle concentration, at lower sticky end coverage, and whenever the overall bead−bead binding free energy is less negative, e.g., due to weaker interparticle bridges. Our simple quantitative model, in which we subsequently apply eqs 11 and 14, 13 and 17, 9, 8, and 18, satisfactorily reproduces the characteristic association−dissociation kinetics observed for different types of DNA constructs and provides insight into the underlying hybridization events (refer to ref 17 for the expressions that describe the *equilibrium* dissociation transition of the beads). The associated configurational entropy costs are difficult to predict a priori, but once they have been determined for a particular experimental system they can be used to predict the behavior for similar systems and for the same system under different conditions. We do observe some dependence of the configurational entropy costs on the sticky end coverage though.

We further find that self-complementary sticky ends readily form intraparticle loops, both with single-stranded and with double-stranded tether backbones, and that these loops dramatically alter the particles' association behavior. For our DNA constructs the configurational entropy cost of the loops is always slightly larger than that of the interparticle bridges, making them suitable for reversible self-protection of the sticky ends.[22]

Optimal self-protection is only achieved, though, when the loops are combined with hairpins, because the latter can protect sticky ends that accidentally remain without a binding partner. We point out that graphs like Figure 9, in which the particles' aggregation rate is plotted as a function of the temperature relative to the solution melting temperature of the most important secondary structures, form a very practical tool for extrapolating the expected effect of self-protection in a certain system without more quantitative modeling. Finally, while the self-protected interactions give a particularly good control over the particles' interactions and their assembly process, the comparative study presented here should also help more generally for designing optimal DNA-mediated self-assembly schemes. Moreover, the observations can be extended to other (biological) systems with, for instance, tethered ligands and receptors.[32,33]

Experimental Section

Our DNA constructs consisted of an 8−11 nucleotide long single-stranded sticky end at the 3′ terminus of a 50 nucleotide long backbone strand (Supporting Information Figure 1) which was attached to a 5′-biotin group through a short, flexible polyethylene glycol spacer. In the double-stranded constructs the backbone was hybridized from its 5′ terminus to a complementary strand of 49 nucleotides long. The backbone hybridization was done in 50 mM phosphate/50 mM NaCl hybridization buffer (pH 7.5) at an overall concentration of 15 μM (UV-260 absorption, Genequant spectrometer) and with a 50% excess of complementary strand by slowly cooling from 90 to 22 °C in a water bath. We purchased the C_N/C'_N oligonucleotides from Integrated DNA Technologies, but synthesized the palindromic sequences ourselves on an Applied Biosystems 394 DNA synthesizer. After completion, we removed the oligonucleotides from the support and deprotected them using routine phosphoramidite procedures.[34] Table 1 lists the enthalpic and entropic contributions to the solution hybridization free energies ($\Delta G^\circ = \Delta H^\circ - T\Delta S^\circ$) of the sticky ends and their secondary structures, as we obtained them from the Mfold Web server,[31] using $[Na^+] = 68$ mM for the suspension buffer.

We functionalized 1.05 μm diameter, streptavidin-coated, paramagnetic polystyrene Dynabeads (MyOne Streptavidin C1, Molecular Probes) with the biotinylated DNA constructs by incubating 5 μL of bead suspension for 30 min at 55 °C with 5 μL of a 6 μM oligonucleotide solution and 65 μL of suspension buffer (10 mM phosphate/50 mM NaCl and 0.5% (w/w) Pluronic surfactant F127, pH 7.5). To remove excess and nonspecifically adsorbed DNA, we centrifuged and resuspended the particles three times in 100 μL of suspension buffer; we repeated this washing procedure twice, heating in between for 30 min at 55 °C. For both the double-stranded and single-stranded constructs we determined the surface coverage to be $N_{total} \approx 15\,500$ strands per particle by means of a separate radioactive labeling experiment.[17] The microscopy samples were made by confining the DNA-functionalized particle suspensions to borosilicate glass capillaries (inner dimensions 2.0 × 0.1 mm, Vitrocom), which first underwent a plasma etching and silanization treatment. The capillary was then mounted on a special stage setup on a Leica DMRXA light microscope, which allowed for fine temperature control, while imaging in transmission mode (see the description in ref 30). The high specific weight of the particles led to fast sedimentation and essentially two-dimensional samples, facilitating the determination of the particle singlet fraction by common video microscopy methods.[35] The surface concentration of the particles was typically around 2.8×10^{11} particles/ m^2, unless indicated otherwise.

Table 1. Thermodynamic Parameters of the Oligonucleotides

structure	ΔH° (kJ/mol)	ΔS° [J/(mol K)]
C_N/C'_N	−370	−1083
P_1	−265	−766
P_2	−277	−789
P_2 hairpin	−75.3	−250
P_3	−296	−841
P_3 hairpin 1	−84.9	−276
P_3 hairpin 2	−148	−472

Acknowledgment. We thank D. Frenkel and M. Zuker for useful discussions. This work was supported partially by the MRSEC Program of the National Science Foundation under Award Number DMR-0820341, by the Keck Foundation, and by The Netherlands Organisation for Scientific Research (NWO).

Supporting Information Available: Additional equations of our theoretical model and an overview of the DNA constructs that were used in the experiments. This material is available free of charge via the Internet at http://pubs.acs.org.

JA907919J

(32) Moore, N. W.; Kuhl, T. L. *Biophys. J.* **2006**, *91*, 1675–1687.
(33) Bongrand, P. *Rep. Prog. Phys.* **1999**, *62*, 921–968.
(34) Caruthers, M. H. *Science* **1985**, *230*, 281–285.
(35) Crocker, J. C.; Grier, D. *J. Colloid Interface Sci.* **1996**, *179*, 298–310.